

# Visible-Light-Induced Electron Transport from Small to Large Nanoparticles in Bimodal Gold Nanoparticle-Loaded Titanium(IV) Oxide\*\*

Shin-ichi Naya, Tadahiro Niwa, Takahiro Kume, and Hiroaki Tada\*

**Abstract:** A key to realizing the sustainable society is to develop highly active photocatalysts for selective organic synthesis effectively using sunlight as the energy source. Recently, metal-oxide-supported gold nanoparticles (NPs) have emerged as a new type of visible-light photocatalysts driven by the excitation of localized surface plasmon resonance of Au NPs. Here we show that visible-light irradiation ( $\lambda > 430$  nm) of TiO<sub>2</sub>-supported Au NPs with a bimodal size distribution (BM-Au/TiO<sub>2</sub>) gives rise to the long-range ( $> 40$  nm) electron transport from about 14 small (ca. 2 nm) Au NPs to one large (ca. 9 nm) Au NP through the conduction band of TiO<sub>2</sub>. As a result of the enhancement of charge separation, BM-Au/TiO<sub>2</sub> exhibits a high level of visible-light activity for the one-step synthesis of azobenzenes from nitrobenzenes at 25 °C with a yield greater than 95 % and a selectivity greater than 99 %, whereas unimodal Au/TiO<sub>2</sub> (UM-Au/TiO<sub>2</sub>) is photocatalytically inactive.

The discovery of the high thermocatalytic activities of Au NPs for many chemical reactions has made us perceive the importance of their size control in a nanoscale range.<sup>[1]</sup> Au NPs also possess unique absorption due to the localized surface plasmon resonance (LSPR) in the whole visible region.<sup>[2]</sup> From a viewpoint of the effective solar energy utilization, Au NP-loaded metal oxides (Au/MOs) have recently attracted much interest as a new type of visible-light photocatalysts, so-called “plasmonic photocatalyst”.<sup>[3–5]</sup> The LSPR excitation of Au/MOs induces oxidation ability on the Au surface because of the interfacial electron transfer (IET) from Au NP to the conduction band (CB) of MO.<sup>[6,7]</sup> The representative “plasmonic photocatalysts” is Au/TiO<sub>2</sub>, which has so far been applied for the oxidative organic transformations including alcohols to aldehydes,<sup>[8–10]</sup> thiols to disulfides,<sup>[11]</sup> benzene to phenol,<sup>[12,13]</sup> and amines to imines.<sup>[14]</sup> A major challenge of the Au/TiO<sub>2</sub> plasmonic photocatalyst is

enhancing the charge separation to effectively use the photo-generated charge carriers for surface reactions.<sup>[15,16]</sup> Also, the extension of its applicability to the reductive organic synthesis would further increase the value. Azobenzenes are usually synthesized by the reduction of nitrobenzenes to anilines, and subsequent diazo-coupling or oxidative coupling.<sup>[17]</sup> Azobenzene derivatives are widely used for pigments, food additives, pharmaceuticals, and can also be applied to the optical switching and storage devices owing to the photochromism.<sup>[18]</sup> The conventional synthetic processes of azobenzenes require the stoichiometric amount of the reagents with the generation of a large amount of wastes. A clean process using Au/TiO<sub>2</sub> as a thermocatalyst has recently been developed for the selective reduction of nitrobenzenes to azobenzenes.<sup>[19]</sup> However, high pressure hydrogen (9 bar) and temperature (120 °C) are necessary for the two step reaction to proceed. On the other hand, UV-light photocatalytic reduction of nitrobenzene by TiO<sub>2</sub>,<sup>[20]</sup> Ag/TiO<sub>2</sub><sup>[21]</sup> and Au/TiO<sub>2</sub><sup>[22]</sup> has so far been studied by many research groups.

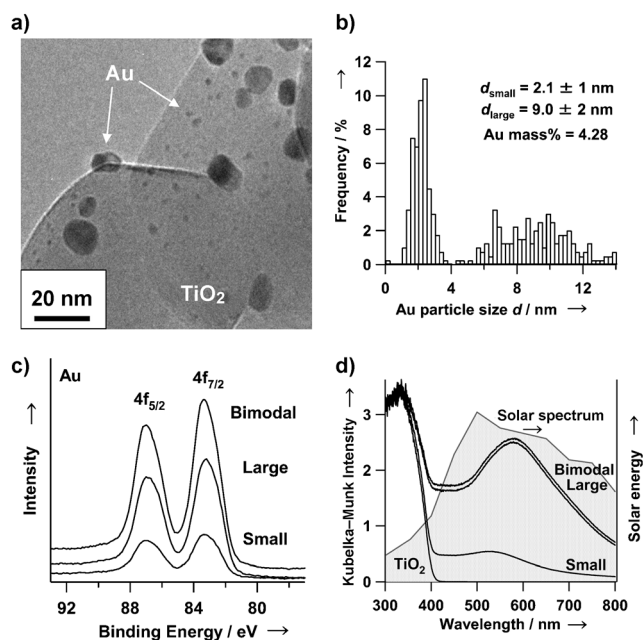
Herein, we present a new strategy for the enhancement of the visible-light-driven charge separation of the Au/TiO<sub>2</sub> plasmonic photocatalyst and its applicability for the reductive organic synthesis by modifying the Au NP size distribution on the TiO<sub>2</sub> surface. BM-Au/TiO<sub>2</sub> has been prepared by a two-step route consisting of the deposition-precipitation and the chemical reduction. The reduction of nitrobenzene derivatives has been performed in the presence of Au/TiO<sub>2</sub> at 25 °C. The LSPR excitation-induced electron transport between small and large Au NPs has been studied by photoelectrochemical measurements, the visualization of redox sites by the CdS photodeposition<sup>[23]</sup> and the photoinduced dissolution and redeposition of Au NPs on TiO<sub>2</sub>.<sup>[24]</sup>

UM- and BM-Au/TiO<sub>2</sub> photocatalysts were prepared as follows. At the first step, large Au NPs were loaded on rutile TiO<sub>2</sub> (L-Au/TiO<sub>2</sub>) by the deposition-precipitation method.<sup>[25]</sup> At the second step, [Au(OH)<sub>3</sub>Cl]<sup>–</sup> complex ions were adsorbed on the TiO<sub>2</sub> surface of the L-Au/TiO<sub>2</sub>, and then, they were reduced by NaBH<sub>4</sub> to yield small Au NPs. For comparison, the second procedure was also applied to unmodified TiO<sub>2</sub> to produce small Au NP-loaded TiO<sub>2</sub> (S-Au/TiO<sub>2</sub>). The physical properties of BM- and UM-Au/TiO<sub>2</sub> are summarized in Table S1. Figure 1 a shows a transmission electron micrograph (TEM) of BM-Au/TiO<sub>2</sub>. S- and L-Au NPs are separately loaded on the same TiO<sub>2</sub> particle in a high dispersion state. The distance between L-Au NP and neighboring S-Au NPs ranges from 1 to 40 nm (see Figure S1 in the Supporting Information). High-resolution TEM shows the intimate contact between Au NP and TiO<sub>2</sub> with a large contact area (Figure S2). Figure 1 b shows the Au particle size

[\*] Dr. S. Naya, Prof. Dr. H. Tada  
Environmental Research Laboratory, Kinki University  
3-4-1, Kowakae, Higashi-Osaka, Osaka 577-8502 (Japan)  
T. Niwa, T. Kume, Prof. Dr. H. Tada  
Department of Applied Chemistry  
School of Science and Engineering, Kinki University  
3-4-1, Kowakae, Higashi-Osaka, Osaka 577-8502 (Japan)  
E-mail: h-tada@apch.kindai.ac.jp

[\*\*] This work was partially supported by a Grant-in-Aid for Scientific Research (C) (grant number 24550239), the Nippon Sheet Glass Foundation for Materials Science and Engineering, and the Sumitomo Foundation.

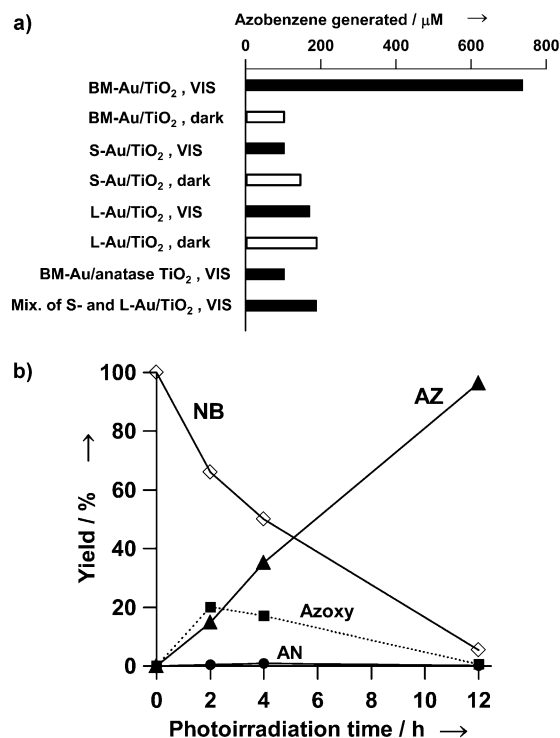
Supporting information for this article is available on the WWW under <http://dx.doi.org/10.1002/anie.201402939>.



**Figure 1.** a) TEM image of BM-Au/TiO<sub>2</sub>. b) Au particle size distribution and its loading amount for BM-Au/TiO<sub>2</sub>. c) Au 4f X-ray photoelectron spectra of Au/TiO<sub>2</sub>. d) UV/Vis absorption spectra of Au/TiO<sub>2</sub> and TiO<sub>2</sub> and the solar spectrum.

distribution of BM-Au/TiO<sub>2</sub> with a loading amount of 4.28 mass %. The  $d$  values of S- and L-Au NPs are 2.1 nm and 9.0 nm, respectively. The loading amounts of S(0.64 mass %)- and L(3.64 mass %)-Au NPs were controlled to balance the surface areas of S(0.95 m<sup>2</sup> g<sup>-1</sup>)- and L(1.26 m<sup>2</sup> g<sup>-1</sup>)-Au NPs. Figure 1c shows the Au 4f-X-ray photoelectron spectra of Au/TiO<sub>2</sub>. In every sample, the signals are present at 87.0 and 83.3 eV, which are in agreement with the values for the Au 4f<sub>5/2</sub> and Au 4f<sub>7/2</sub> of metallic Au, respectively. Thus, the Au<sup>III</sup> complex adsorbed on TiO<sub>2</sub> is reduced to metallic Au by NaBH<sub>4</sub> at the second step. Figure 1d shows UV-visible absorption spectra of Au/TiO<sub>2</sub> and TiO<sub>2</sub>, and the solar spectrum. Au/TiO<sub>2</sub> samples have broad LSPR-absorption around 550 nm, of which profile well resembles that of the solar spectrum.

The thermo- and photo-catalytic activities of BM- and UM-Au/TiO<sub>2</sub> for the reduction of nitrobenzene were studied at 25 °C in the dark and under visible-light irradiation ( $\lambda > 430$  nm), respectively. Figure 2a compares the yields of azobenzene under anaerobic conditions at reaction time of 2 h. Every Au/TiO<sub>2</sub> has a thermocatalytic activity for the reduction of nitrobenzene to azobenzene. UM-Au/TiO<sub>2</sub> is photocatalytically inactive, since the amount of azobenzene is comparable with that obtained in the dark. Surprisingly, BM-Au/TiO<sub>2</sub> exhibits a high visible-light activity much greater than the physical mixture of S-Au/TiO<sub>2</sub> and L-Au/TiO<sub>2</sub>. The turnover number ( $= 2 \times$  number of azobenzene produced/number of surface Au atoms) reaches 520 at 12 h. No azobenzene was produced under aerobic conditions. The activity of BM-Au/TiO<sub>2</sub> strongly depends on the crystal form of TiO<sub>2</sub>, that is, BM-Au/anatase TiO<sub>2</sub> is lower than that of BM-Au/rutile TiO<sub>2</sub>. This remarkable difference stems from

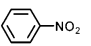
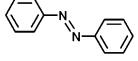

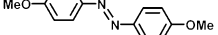
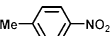
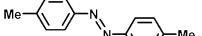
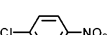
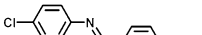
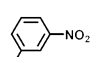
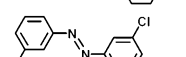


**Figure 2.** a) Azobenzene formed at reaction time = 2 h by using various Au/TiO<sub>2</sub>. b) Time courses for nitrobenzene reduction by BM-Au/TiO<sub>2</sub>: nitrobenzene (NB,  $\diamond$ ), azobenzene (AZ,  $\blacktriangle$ ), azoxybenzene (Azoxy,  $\blacksquare$ ), aniline (AN,  $\bullet$ ). Reaction conditions: BM-Au/TiO<sub>2</sub> 10 mg, nitrobenzene (10 mM) solution (10 mL, 2-propanol) with KOH (10 mM), visible-light ( $\lambda > 430$  nm, 10 mW cm<sup>-2</sup>) irradiation at 25 °C under anaerobic conditions.

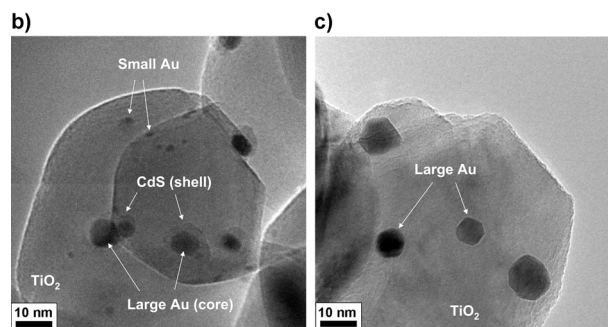
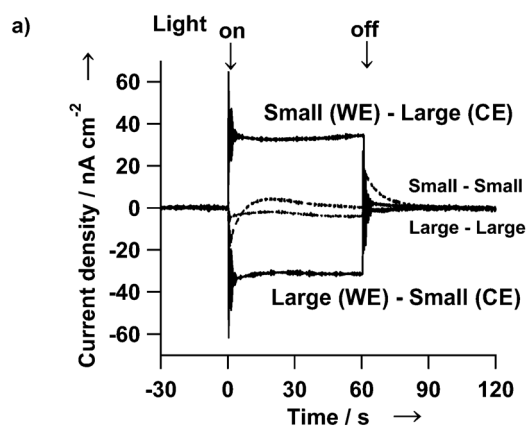
the larger permittivity of rutile TiO<sub>2</sub> ( $\epsilon = 114$ ) than anatase TiO<sub>2</sub> ( $\epsilon = 48$ ), which leads to the higher activity of the Au/TiO<sub>2</sub> plasmonic photocatalyst for the oxidation of alcohol.<sup>[26]</sup> Figure 2b shows the time course for the nitrobenzene reduction in the BM-Au/rutile TiO<sub>2</sub> system. The yield of azobenzene increases with increasing irradiation time to reach 95 % at 12 h with a selectivity greater than 99 %, and acetone was generated as a result of the 2-propanol oxidation. Azoxybenzene is transiently generated, while the amount of aniline is negligibly small. The reaction started by an azoxybenzene solution quantitatively afforded azobenzene, whereas the reaction with a mixed solution of 5 mM nitrobenzene and 5 mM aniline only produced 2.5 mM azobenzene. Thus, this reaction would proceed via azoxybenzene as an intermediate. Table 1 shows the results on the BM-Au/TiO<sub>2</sub>-photocatalyzed reduction of nitrobenzene derivatives. Every nitrobenzene derivative is reduced to the corresponding azobenzene derivative with a conversion greater than 95 % and a selectivity greater than 99 %.

Mesoporous films comprising of UM-Au/TiO<sub>2</sub> particles were formed on indium-tin oxide film-coated glass plates (Au/TiO<sub>2</sub>/ITO). To clarify the origin for the high visible-light activity of BM-Au/TiO<sub>2</sub>, photoelectrochemical measurements were performed for the electrodes. Figure 3a shows the photochronoamperometry profiles for the two electrode systems in an electrolyte solution containing 2-propanol.

**Table 1:** BM-Au/TiO<sub>2</sub>-photocatalyzed reduction of nitrobenzenes (Conv. = conversion and Selec. = selectivity).<sup>[a]</sup>

Substrate	Product	t [h]	Conv. [%]	Selec. [%]
		12	95	> 99
		24	> 99	> 99
		20	98	> 99
		24	> 99	> 99
		12	> 99	> 99

[a] Reaction conditions: BM-Au/TiO<sub>2</sub> 10 mg, nitrobenzene (10 mM) solution (10 mL, 2-propanol) with KOH (10 mM), visible-light ( $\lambda > 430$  nm, 10 mW cm<sup>-2</sup>) irradiation at 25 °C under anaerobic conditions.



**Figure 3.** a) Photochronoamperometry profiles for the two electrode system employing S-Au/TiO<sub>2</sub>/ITO and L-Au/TiO<sub>2</sub>/ITO as working electrode (WE) and counter electrode (CE) in an electrolyte solution containing 2-propanol under simultaneous illumination ( $\lambda > 430$  nm) of both electrodes at the dark rest potential. b) TEM image for BM-Au/TiO<sub>2</sub> with CdS photodeposited by visible-light irradiation ( $\lambda > 430$  nm). c) TEM image for BM-Au/TiO<sub>2</sub> after irradiation ( $\lambda > 430$  nm) in a 1 M NaCl aqueous solution.

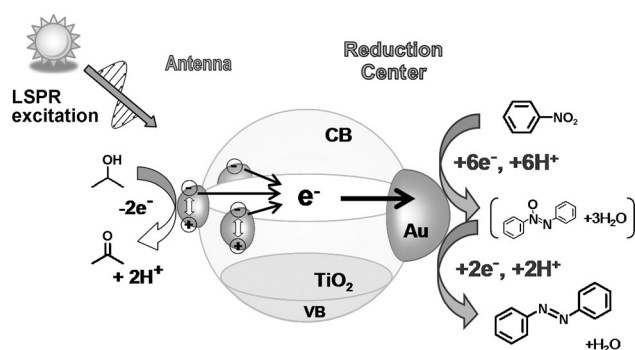
Simultaneous visible-light irradiation ( $\lambda > 430$  nm) of the asymmetrical cell using S-Au/mp-TiO<sub>2</sub>/ITO and L-Au/mp-TiO<sub>2</sub>/ITO as working electrode (WE) and counter electrode (CE), respectively, generates an anodic current. On exchanging the electrodes (L-Au/TiO<sub>2</sub>/ITO for WE and S-Au/TiO<sub>2</sub>/

ITO for CE), the polarity of the photocurrent is reversed. On the other hand, the symmetrical cell with two S-Au/TiO<sub>2</sub>/ITO (or L-Au/TiO<sub>2</sub>/ITO) electrodes as WE and CE yields no stationary current. These results strongly suggest that the net electron transport from S- to L-Au NPs through the CB(TiO<sub>2</sub>) is induced in BM-Au/TiO<sub>2</sub> by the LSPR excitation [Eq. (S1)].

CdS is deposited on Au/TiO<sub>2</sub> by UV-light irradiation in a solution containing Cd<sup>2+</sup> ions and S<sub>8</sub>.<sup>[23]</sup> The CdS photodeposition selectively occurs on the surface of electron rich Au NPs (or the reduction sites) to yield Au(core)-CdS(shell) nanocrystals on TiO<sub>2</sub>, and thus, the reduction sites of BM-Au/TiO<sub>2</sub> can be visualized by taking advantage of this reaction. Figure 3b shows a TEM image for BM-Au/TiO<sub>2</sub> with CdS photodeposited by visible-light irradiation ( $\lambda > 430$  nm). CdS shells are formed on not S- but L-Au NPs. Also, the photoinduced dissolution and redeposition of Au NPs loaded on TiO<sub>2</sub> in aqueous solutions of metal halides<sup>[24]</sup> can be utilized to specify the electron poor Au NPs (or the oxidation sites). Figure 3c shows a TEM image for BM-Au/TiO<sub>2</sub> after visible-light ( $\lambda > 430$  nm) in a 1 M NaCl aqueous solution irradiation for 1 h. All the S-Au NPs disappear, while L-Au NPs grow. These results verify that the surfaces of L- and S-Au NPs act as the reduction sites [Eqs. (S2) and (S3)] and oxidation ones [Eqs. (S4) and (S5)], respectively.

The electrons in both S- and L-Au NPs are pumped up to the CB(TiO<sub>2</sub>) by the LSPR excitation of Au/TiO<sub>2</sub>.<sup>[6,7]</sup> and the Fermi energy of the Au NPs lowers. The number of Au atoms in one S-Au NP is smaller than that in one L-Au NP by two orders of magnitude. Because of the smaller density of states for the S-Au NP, the Fermi energy at the photostationary state  $E_F^*$  of S-Au NP effectively lowers with the IET to reach the oxidation potential of 2-propanol (+0.32 V vs. standard hydrogen electrode, SHE).<sup>[27]</sup> As a result, 2-propanol is oxidized on the surface of S-Au NP. On the other hand, the electron capturing ability of Au NPs from the CB(TiO<sub>2</sub>) increases with an increase in  $d$  at  $< 13$  nm.<sup>[28]</sup> The alleviation of the electron-electron repulsion in a wider space could permit for L-Au NP to accept the excess electrons from the CB(TiO<sub>2</sub>). Consequently, the  $E_F^*$  of L-Au NP attains the reduction potential of nitrobenzene (−1.09 V vs. SHE),<sup>[29]</sup> which is reduced on the surface. Energetically, the LSPR excitation (2.25 eV) can drive the vectorial electron transport from S- to L-Au NPs against the energy difference between the  $E_F^*$  values of S- and L-Au NPs (ca. 1.4 eV).

On the basis of these results, we present a reaction mechanism in Scheme 1. Nitrobenzene has an n- $\pi^*$  transition absorption band centered at 266 nm, but no absorption in the visible region. The LSPR excitation of BM-Au/TiO<sub>2</sub> causes the net electron transport from S- to L-Au NPs through the CB(TiO<sub>2</sub>). The intimate contact between Au NPs and TiO<sub>2</sub> with a large contact area of Au/TiO<sub>2</sub> would be favorable for the IET. As a result of the long-range charge separation reaching over about 40 nm, the surfaces of S- and L-Au NPs efficiently operate as the oxidation and reduction sites, respectively. In this case, one L-Au NP receives electrons from about 14 S-Au NPs on the average. Interestingly, this electron-harvesting mechanism is analogous to the mechanism on the energy transfer from antenna chlorophyll to P680 in the photosystem II of natural photosynthesis. The fairly



Scheme 1. Reaction mechanism.

weak visible-light absorption of S-Au NPs can be compensated by their cooperation. Nitrobenzene is strongly adsorbed through the nitro group at the interface between the Au NP and TiO<sub>2</sub>.<sup>[30]</sup> In those sites around L-Au NPs, nitrobenzene undergoes eight-electron reduction to azobenzene via azoxybenzene by their electron pool effect. On the other hand, 2-propanol is oxidized to acetone on the surface of S-Au NPs. Recently, selective reduction of nitrobenzene to azobenzene has been reported by visible-light irradiation of Au/ZrO<sub>2</sub> at intense light intensity (ca. 300 mW cm<sup>-2</sup>) and 40 °C.<sup>[31]</sup> The reaction mechanism should be different from that in this system because the LSPR excitation-induced IET from Au NP to the very higher lying CB(ZrO<sub>2</sub>) cannot occur.<sup>[7]</sup> Consequently, the high visible-light activity of BM-Au/TiO<sub>2</sub> is ascribable to the enhancement of charge separation by the net one-directional electron transport from S- to L-Au NPs.

BM-Au/TiO<sub>2</sub> with mean small and large particle sizes of about 2 nm and 9 nm, respectively, has been prepared by a two-step route consisting of the deposition-precipitation and the chemical reduction. Visible-light irradiation ( $\lambda > 430$  nm) of BM-Au/rutile TiO<sub>2</sub> induces the net electron transport from small to large Au NPs through the conduction band of TiO<sub>2</sub>. Because of the resulting enhancement in the charge separation, BM-Au/rutile TiO<sub>2</sub> exhibits a very high level of visible-light activity for the reductions of nitrobenzene derivatives, whereas UM-Au/rutile TiO<sub>2</sub> only has a low thermocatalytic activity. The corresponding azobenzene derivatives are produced with conversion greater than 95% and selectivity greater than 99% at 25 °C. Meanwhile the design of the experimental equipment and setup for scaling-up of the products is practically important, we anticipate that the present strategy is widely applicable to the plasmon photocatalysts with various metal and semiconductor components, and further open up a new avenue for their applications to not only oxidative but also reductive syntheses of important chemical compounds.

## Experimental Section

**Catalyst preparation and characterization:** At the first step, L-Au/TiO<sub>2</sub> was prepared by the deposition-precipitation method using HAuCl<sub>4</sub> and urea as a starting material and a neutralizer, respectively. The post-heating was carried out at 600 °C for 4 h. L-Au/TiO<sub>2</sub> (2 g) was added to a 4.86 mM aqueous solution of HAuCl<sub>4</sub> neutralized by

NaOH, and then, the suspension was heated at 70 °C for 1 h. The particles were washed with distilled water to be dried under vacuum. At the second step, after the particles were re-dispersed in EtOH (60 mL) containing NaBH<sub>4</sub> (11 mg), the suspension was stirred at 25 °C for 1 h. The resulting particles were washed with distilled water, and dried under vacuum (BM-Au/TiO<sub>2</sub>). The second step was applied to unmodified TiO<sub>2</sub> to prepare small Au NP-loaded TiO<sub>2</sub>. The mean size of the Au NPs was determined by transmission electron microscopy at an applied voltage of 300 kV (JEM-3010, JEOL). The Au loading amount was quantified by inductively coupled plasma spectroscopy (ICPS-7500, Shimadzu). Diffuse reflectance UV-Vis-NIR spectra of the samples were recorded on a Hitachi U-4000 spectrometer mounted with an integrating sphere at room temperature. The reflectance ( $R_{\infty}$ ) was recorded with respect to a reference of BaSO<sub>4</sub>, and the Kubelka-Munk function [ $F(R_{\infty})$ ] expressing the relative absorption coefficient was calculated by the equation  $F(R_{\infty}) = (1 - R_{\infty})^2 / 2R_{\infty}$ . X-ray photoelectron spectroscopic (XPS) measurements were performed using a Kratos Axis Nova X-ray photoelectron spectrometer with a monochromated Al K $\alpha$  X-ray source operated at 15 kV and 10 mA using C1s as the energy reference (284.6 eV).

**Reduction of nitrobenzene derivatives:** The suspension of Au/TiO<sub>2</sub> (10 mg) in a 2-propanol solution of nitrobenzene (10 mm, 10 mL) with KOH (10 mm) was degassed by saturation with argon for 30 minutes in the dark. Irradiation was started using a 300 W Xe lamp (HX-500, Wacom) with a cut off filter Y-45 (AGC TECHNO GLASS) in a double jacket type reaction cell (18 mm in diameter and 180 mm in length). The light intensity integrated from 420 to 485 nm ( $I_{420-485}$ ) through a Y-45 optical filter was adjusted to 10.0 mW cm<sup>-2</sup>. The yield and selectivity were determined by high-performance liquid chromatography (LC-6 AD, SPD-6A, C-R8A (Shimadzu)) [measurement conditions: column = Shim-pack CLC-ODS (4.6 mm  $\times$  150 mm) (Shimadzu); MeOH:H<sub>2</sub>O = 7:3; flow rate = 1.0 mL min<sup>-1</sup>;  $\lambda$  = 240 nm].

**Photoelectrochemical measurements:** A slurry of Au/TiO<sub>2</sub> (0.5 g) in H<sub>2</sub>O (1 mL) with acetylacetone (50 mg) and polyethylene glycol 20000 (0.25 g) was coated on ITO-film coated glass substrates (sheet resistance = 12  $\Omega$  per square), and the samples were heated in air at 773 K for 1 h to form Au/mp-TiO<sub>2</sub>/ITO electrodes [The mean size of small Au particles increased from 2.1 to 4.3 nm (Figure S4), which was still sufficiently smaller as compared to the mean size of large Au particles (9.0 nm)]. The electrochemical cells comprising of the photoanode | 5% 2-propanol + 0.1M Na<sub>2</sub>SO<sub>4</sub> (aqueous electrolyte solution) | photocathode were fabricated. The active area of the cell was 3.0  $\times$  2 cm<sup>2</sup>. Under illumination by a 300 W Xe lamp (HX-500, Wacom) with a cut off filter Y-45 (AGC TECHNO GLASS), the current density (nA cm<sup>-2</sup>) was measured at the dark rest potential by using a galvanostat/potentiostat (HZ-5000, Hokuto Denko).

**CdS photodeposition on BM-Au/TiO<sub>2</sub>:** A 2-propanol suspension (10 mL) containing BM-Au/TiO<sub>2</sub> particles (20 mg), S<sub>8</sub> (13.8 mm) and Cd(ClO<sub>4</sub>)<sub>2</sub> (13.8 mm) was bubbled with argon for 0.5 h in the dark. Visible-light irradiation was carried out for 24 h using a 300 W Xe lamp (HX-500, Wacom) with a cut off filter Y-45 (AGC TECHNO GLASS) in a double jacket type reaction cell (18 mm in diameter and 180 mm in length). The light intensity integrated from 420 to 485 nm ( $I_{420-485}$ ) through a Y-45 optical filter was adjusted to 3 mW cm<sup>-2</sup>. After irradiation, the particles were recovered by centrifugation, and the resulting particles were washed with ethanol three times to be dried under vacuum.

Received: March 3, 2014

Revised: April 13, 2014

Published online: May 26, 2014

**Keywords:** gold · nanoparticles · photocatalysis · surface plasmon resonances · visible light

- [1] M. Haruta, *Nature* **2005**, 437, 1098–1099.
- [2] G. V. Hartland, *Chem. Rev.* **2011**, 111, 3858–3887.
- [3] A. Kubacka, M. Fernandez-Garcia, G. Colon, *Chem. Rev.* **2012**, 112, 1555–1614.
- [4] K. Ueno, H. Misawa, *J. Photochem. Photobiol. C* **2013**, 15, 31–52.
- [5] X. Lang, X. Chen, J. Zhao, *Chem. Soc. Rev.* **2014**, 43, 473–486.
- [6] Y. Tian, T. Tatsuma, *J. Am. Chem. Soc.* **2005**, 127, 7632–7637.
- [7] A. Furube, L. Du, K. Hara, R. Katoh, M. Tachiya, *J. Am. Chem. Soc.* **2007**, 129, 14852–14853.
- [8] E. Kowalska, R. Abe, B. Ohtani, *Chem. Commun.* **2009**, 241–243.
- [9] S. Naya, A. Inoue, H. Tada, *J. Am. Chem. Soc.* **2010**, 132, 6292–6293.
- [10] D. Tsukamoto, Y. Shiraishi, Y. Sunagano, S. Ichikawa, S. Tanaka, T. Hirai, *J. Am. Chem. Soc.* **2012**, 134, 6309–6315.
- [11] S. Naya, M. Teranishi, T. Isobe, H. Tada, *Chem. Commun.* **2010**, 46, 815–817.
- [12] Y. Ide, M. Matsuoka, M. Ogawa, *J. Am. Chem. Soc.* **2010**, 132, 16762–16764.
- [13] Z. Zheng, B. Huang, X. Qin, X. Zhang, Y. Dai, M.-H. Whangbo, *J. Mater. Chem.* **2011**, 21, 9079–9087.
- [14] S. Naya, K. Kimura, H. Tada, *ACS Catal.* **2013**, 3, 10–13.
- [15] X. Wu, E. S. Thrall, M. Steigerwald, L. Brus, *J. Phys. Chem. C* **2010**, 114, 12896–12899.
- [16] Z. Bian, T. Tachikawa, P. Zhang, M. Fujitsuka, T. Majima, *J. Am. Chem. Soc.* **2014**, 136, 458–465.
- [17] M. B. Smith, J. March, *March's advanced organic chemistry 6th Revised*, Wiley, Hoboken, **2007**.
- [18] H. M. Dhammika Bandara, S. C. Burdette, *Chem. Soc. Rev.* **2012**, 41, 1809–1825.
- [19] A. Grirrane, A. Corma, H. Garcia, *Science* **2008**, 322, 1661–1664.
- [20] a) F. Mahdavi, T. C. Bruton, Y. Li, *J. Org. Chem.* **1993**, 58, 744–746; b) J. L. Ferry, W. H. Glaze, *Langmuir* **1998**, 14, 3551–3555; c) H. Kominami, S. Iwasaki, T. Maeda, K. Imamura, K. Hashimoto, Y. Kera, B. Ohtani, *Chem. Lett.* **2009**, 38, 410–411; d) A. Hakki, R. Dillert, D. Bahnemann, *Catal. Today* **2009**, 144, 154–159; e) Y. Shiraishi, H. Hirakawa, Y. Togawa, Y. Sugano, S. Ichikawa, T. Hirai, *ACS Catal.* **2013**, 3, 2318–2326; f) L. Liu, X. Gu, Z. Ji, W. Zou, C. Tang, F. Gao, L. Dong, *J. Phys. Chem. C* **2013**, 117, 18578–18587.
- [21] a) H. Tada, T. Ishida, A. Takao, S. Ito, *Langmuir* **2004**, 20, 7898–7900; b) H. Tada, T. Ishida, A. Takao, S. Ito, S. Mukhopadhyay, T. Akita, K. Tanaka, H. Kobayashi, *ChemPhysChem* **2005**, 6, 1537–1543.
- [22] T. Kiyonaga, M. Fujii, T. Akita, H. Kobayashi, H. Tada, *Phys. Chem. Chem. Phys.* **2008**, 10, 6553–6561.
- [23] H. Tada, T. Mitsui, T. Kiyonaga, T. Akita, K. Tanaka, *Nat. Mater.* **2006**, 5, 782–786.
- [24] T. Kawahara, T. Soejima, T. Mitsui, T. Kiyonaga, H. Tada, S. Ito, *J. Colloid Interface Sci.* **2005**, 286, 816–819.
- [25] R. Zanella, L. Delannoy, C. Louis, *Appl. Catal. A* **2005**, 291, 62–72.
- [26] K. Kimura, S. Naya, Y. Jin-nouchi, H. Tada, *J. Phys. Chem. C* **2012**, 116, 7111–7117.
- [27] J. Ye, J. Liu, C. Xu, S. P. Jiang, Y. Tong, *Electrochem. Commun.* **2007**, 9, 2760–2763.
- [28] T. Tada, T. Kiyonaga, S. Naya, *Chem. Soc. Rev.* **2009**, 38, 1849–1858.
- [29] A. Kuhn, K. G. von Eschwege, J. Conradie, *J. Phys. Org. Chem.* **2012**, 25, 58–68.
- [30] M. Boronat, P. Concepción, A. Corma, S. González, F. Illas, P. Serna, *J. Am. Chem. Soc.* **2007**, 129, 16230–16237.
- [31] H. Zhu, X. Ke, X. Yang, S. Sarina, H. Liu, *Angew. Chem.* **2010**, 122, 9851–9855; *Angew. Chem. Int. Ed.* **2010**, 49, 9657–9661.